Laser Scanner Jitter Characterization*

Yi-Ting Chen [a], Terry Nelson [b], Tami Ogle [b], Hong Ren [b], Mark Shaw [b], and Jan P. Allebach [a]; a: School of Electrical and Computer Engineering, Purdue University, West Lafayette, Indiana USA; b: Hewlett-Packard Company, Boise, Idaho USA

Abstract

The electrophotographic (EP) process is widely used in imaging systems such as laser printers and office copiers. In the EP process, laser scanner jitter is a common artifact that mainly appears along the scan direction due to the condition of polygon facets. Prior studies have not focused on the periodic characteristic of laser scanner jitter in terms of the modeling and analysis. This paper addresses the periodic characteristic of laser scanner jitter in the mathematical model. In the Fourier domain, we derive an analytic expression for laser scanner jitter in general, and extend the expression assuming a sinusoidal displacement. This leads to a simple closed-form expression in terms of Bessel functions of the first kind. We further examine the relationship between the continuous-space halftone image and the periodic laser scanner jitter. The simulation results show that our proposed mathematical model predicts the phenomenon of laser scanner jitter effectively, when compared to the characterization using a test pattern, which consists of a flat field with 25% dot coverage.

Introduction

The electrophotographic (EP) process is widely used in imaging systems, such as laser printers and office copiers. In the EP process, the overall print quality is determined by the stability of the imaging process. Different mechanical issues contribute to various image artifacts such as fine-pitch banding and laser scanner jitter. Fine-pitch banding is analogous to laser scanner jitter. The only difference being in the direction in which it occurs: fine-pitch banding is due to fluctuations in the process direction, and laser scanner jitter is due to fluctuations in the scan direction. Fine-pitch banding has been widely studied [2, 3, 4]. However, little work has been done on laser scanner jitter in terms of a characterization and analysis that exploits its periodic nature.

A few studies on laser scanner jitter have focused on its root cause [5], ways to reduce it [6], and its characterization [7, 8]. Horikawa et al [5] demonstrated that laser scanner jitter has two typical root causes: rotational variation of the spindle motor and the condition of the facets of the polygon mirror. The first cause is directly related to the rotation speed of the polygon mirror. Therefore, the non-regular variation of the spindle motor influences the low-frequency jitter components in the frequency domain. On the other hand, the condition of the facets of the polygon mirror introduces high-frequency jitter components [5]. Horikawa et al. demonstrated that the high-frequency jitter components were essentially caused by the radius variation of the mirror facets and the curve of the mirror facets [5]. To reduce the effect of laser scanner jitter, Stutz presented a pixel placement correction system, which contains an encoder or clock track to examine the position of the scanner [6].

*Research supported by the Hewlett-Packard Company, Palo Alto, CA.

As for the characterization aspect, Eid et al [7, 8] proposed a characterization method that combined two-dimensional analysis of Gabor pre-filtering to detect and localize the artifacts, and spectral analysis. However, the root cause in [7, 8] is due to oscillatory disturbances of the OPC drum and developer roller. This is different from the causes of the jitter examined in the papers [5, 6]. Most importantly, Eid et al [7, 8] did not investigate the periodic characteristic of laser scanner jitter in their analysis.

In this paper, we focus on laser scanner jitter that is periodic, since the jitter we consider is introduced by the condition of the polygon mirror facets, as discussed in [5, 6]. We present a new method for characterizing the Fourier spectrum of the periodic laser scanner jitter. We view the image as a two-dimensional signal, which has a periodic displacement in the scan direction, and derive an analytic expression for its Fourier spectrum. The laser scanner jitter phenomenon and its periodic characteristic are illustrated in Fig. 1. In Fig. 1, straight lines are printed along the process direction. However, they appear to be wiggly lines instead of straight lines; and we can clearly see the periodic characteristic of the laser scanner jitter. The length of each straight line is 100 printer-addressable pixels or printer scan lines; and the periodic pattern repeats every 10 pixels because the polygon mirror in our target laser printer has 10 facets. Guided by the periodicity of the jitter pattern, we incorporate this characteristic into our mathematical model to more accurately capture the behavior of laser scanner jitter.

In this paper, we mainly focus on characterizing the behavior of the laser scanner jitter, and do not provide a solution to reducing the impact of the jitter in the EP process. The rest of this paper is organized as follows. The next section describes the mathematical model of laser scanner jitter, and then extends the model to the special case where the periodic displacement is a sinusoidal function. Then, we investigate in the Fourier domain the relationship between the halftone image and the periodic laser scanner jitter. Finally, we present an evaluation of the mathematical model and conclusions.

Mathematical Model of Laser Scanner Jitter

We first develop the general mathematical model of periodic laser scanner jitter in a two-dimensional continuous-space for a continuous-tone image, and extend it to the special case of a sinusoidal displacement in the next section. We denote the continuous-tone image by $f(x,y)$. Here x corresponds to the process (vertical) direction, and y corresponds to the scan (horizontal) direction. We define a new image $g(x,y)$, with periodic laser scanner jitter, according to

$$g(x,y) \quad = \quad f\big(x, y - d(x)\big)\,, \tag{1}$$

where the displacement $d(x)$ is periodic in x. Let $F(u,v)$ denote the two-dimensional Continuous-Space Fourier Transform

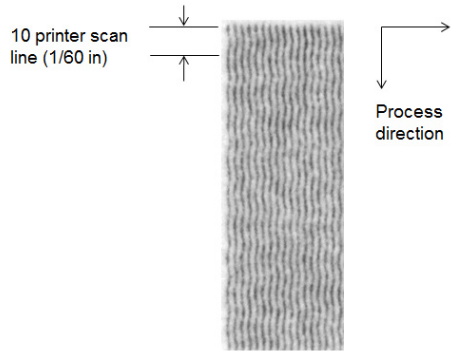

Figure 1. *Straight lines printed in the process direction appear to be wiggly instead of straight. The length of each straight line is* 100 *printer-addressable pixels, and the periodic pattern repeats every 10 pixels because the polygon mirror in our target laser printer has* 10 *facets. The printer resolution is 600 dpi.*

(CSFT) of $f(x,y)$ defined according to

$$F(u,v) = \int_{-\infty}^{+\infty}\int_{-\infty}^{+\infty} f(x,y)e^{-j2\pi(ux+vy)}\mathrm{d}x. \quad (2)$$

Based on the properties of the CSFT, we can derive a closed-form expression for $G(u,v)$ in terms of $F(u,v)$. We have

$$G(u,v) = \sum_k C_k(v)F\left(u-k/X,v\right), \quad (3)$$

where X is the period of the laser scanner jitter, and the Fourier coefficients $C_k(v)$ are given by

$$C_k(v) = \frac{1}{X}\int_{-\frac{X}{2}}^{+\frac{X}{2}} e^{-j2\pi(kx/X+vd(x))}\mathrm{d}x. \quad (4)$$

From Eq. (3), we see that the periodic laser scanner jitter causes replication of the spectrum $F(u,v)$ of the original image in the process (u) frequency direction with interval $\frac{1}{X}$, which is the reciprocal of the period of the jitter. Each replication is weighted differently by a function that varies in the scan (v) frequency direction. Specifically, the k-th replication is weighted by $C_k(v)$.

Periodic Laser Scanner Jitter with Sinusoidal Displacement

In this section, we extend the model to the special case where the periodic displacement is a sinusoid function $d(x) = A\sin(2\pi x/X)$. Here A is a constant scale factor that is the peak jitter displacement, and X is the period of the laser scanner jitter. With an approach similar to that used in the previous section, we can derive the Fourier coefficients as follows

$$C_k(v) = J_k(-2\pi Av), \quad (5)$$

where the Fourier coefficients are articulated by the k-th order Bessel function of the first kind [9].

To obtain the Fourier transform of $g(x,y)$, we substitute Eq. (5) into Eq. (3), yielding

$$G(u,v) = \sum_k J_k(-2\pi Av)F(u-k/X,v). \quad (6)$$

In Eq. (6), the periodic laser scanner jitter introduces replications in the process (u) frequency direction with interval $\frac{1}{X}$. Each replication is weighted by the k-th order Bessel function, $J_k(-2\pi Av)$, that changes in the scan (v) frequency direction. The key difference between Eq. (3) and Eq. (6) is because of the sinusoidal displacement; and we can derive a closed form for Fourier series coefficients, which is the k-th order Bessel function.

To illustrate the structure of the spectrum given by Eq. (6) and in particular, the v-axis dependence of the Fourier coefficients due to the k-th order Bessel function, we use an example in Fig. 2 to demonstrate the phenomena. The image in Fig. $2(a)$ is an infinitely long vertical sinc-strip image $g(x,y) = \mathrm{sinc}(600y)$, where $\mathrm{sinc}(\xi) = \sin(\pi\xi)/(\pi\xi)$. This strip does not vary in the process direction, and is centered at $y = 0$. It has zero crossings spaced apart by $1/600$ inch in the y direction. The Fourier transform of this image is the function $G(u,v) = (1/600)\mathrm{rect}(v/600)\delta(u)$, which is a portion of an impulse sheet oriented along the v-axis. Here, $\mathrm{rect}(\xi) = 1, |\xi| < 1/2$, and $\mathrm{rect}(\xi) = 0$, otherwise. This spectrum is shown in Fig. $2(b)$. Figure $2(c)$ shows the sinc-strip image with laser scanner jitter. The maximum displacement of the jitter is $1/1200$ inches. The Fourier spectrum of the sinc-strip image is shown in Fig. $2(d)$. We can see clearly in Fig. $2(d)$ that the constant amplitude impulse sheet in Fig. $2(b)$ is replicated along the u-axis at multiples of the fundamental frequency 60 cycles/inch of the periodic jitter, and that along the v-axis, the Fourier coefficients $J_k(-2\pi Av)$ continuously modulate the amplitude of each replication of this impulse sheet.

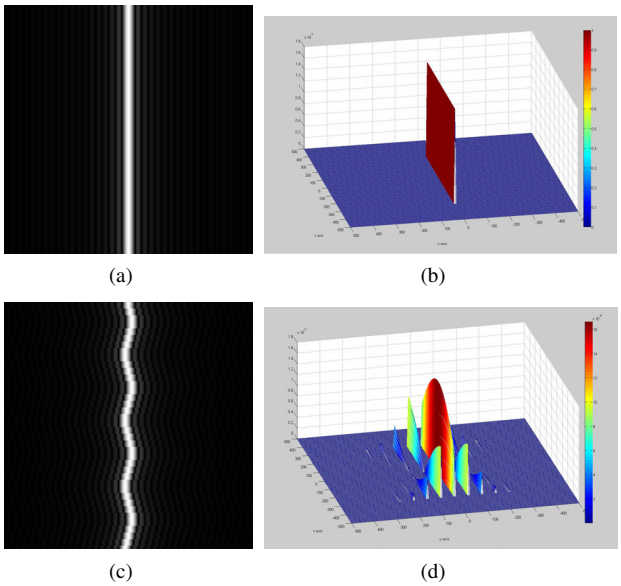

Figure 2. *Illustration of the infinitely long vertical sinc-strip image with laser scanner jitter that shows the v-dependent attenuation in the frequency domain. (a) The infinitely long vertical sinc-strip centered at y = 0 with zero crossings in the y direction separated by* $1/600$ *inch. (b) The Fourier spectrum of the infinitely long vertical sinc-strip image, which is an impulse sheet with a rect function profile along the v-axis. (c) The infinitely long vertical sinc-strip image with laser scanner jitter. (d) The Fourier spectrum of the image in (a) with laser scanner jitter.*

Fourier Analysis of a Halftone Image with Laser Scanner Jitter

In this section, we investigate in Fourier domain the relationship between a halftone image and periodic laser scanner jitter. We first derive in the Fourier domain the halftone image generated by the screening process. We use boldface lower case to represent vectors, and boldface upper case to denote matrices. In the following derivation, we use $(\mathbf{x}) = (x,y)^T$ and $[\mathbf{m}] = [m,n]^T$ to indicate continuous and discrete coordinates, respectively, where the units of $(\mathbf{x})$ and $[\mathbf{m}]$ are inches and printer-addressable pixels, respectively. Here m corresponds to the process (vertical) direction, and n corresponds to the scan (horizontal) direction.

The screening process generates the halftone image by thresholding the discrete-space continuous-tone image with a threshold array. The threshold array is defined by two independent tile vectors $\mathbf{n}_1$ and $\mathbf{n}_2$; and the screen periodicity matrix $\mathbf{N}$ can be written as $\mathbf{N} = [\mathbf{n}_1|\mathbf{n}_2]$. To simplify the derivation, we focus on a constant-tone image for the following analysis. The resulting continuous-space halftone image $h(\mathbf{x};a)$ can be expressed [10] as

$$h(\mathbf{x};a) = \sum_{\mathbf{m}\in Z^2} h[\mathbf{m};a]\; p_{\text{dot}}(\mathbf{x}-\mathbf{m}R)\,, \tag{7}$$

where $h[\mathbf{m};a]$ is the discrete-space halftone image defined as

$$h[\mathbf{m};a] = \begin{cases} 1, & \text{if } a \geq t[\mathbf{m}] \\ 0, & \text{else} \end{cases}, \tag{8}$$

and $p_{\text{dot}}(x)$ is the printer dot profile defined as

$$\begin{aligned} p_{\text{dot}}(\mathbf{x}) &= \text{rect}\,(\mathbf{x}/R)\,, \\ &= \text{rect}(x/R)\text{rect}(y/R)\,. \end{aligned} \tag{9}$$

The variable a is the absorptance between 0 (white) and 1 (black); and the parameter R in Eqs. (7) and (9) is the horizontal and vertical distance between printer-addressable pixels in units of inches.

The CSFT of $h(\mathbf{x};a)$ can be expressed as

$$\begin{aligned} H(\mathbf{u};a) &= \frac{1}{|\mathbf{N}|R} P_{\text{dot}}(\mathbf{u})\breve{C}(\mathbf{u}R;a) \\ &\quad \times \sum_{\mathbf{t}\in Z^2} \delta(\mathbf{u} - \frac{1}{R}\mathbf{N}^{-T}\mathbf{t})\,, \end{aligned} \tag{10}$$

where $P_{\text{dot}}(\mathbf{u})$ is the CSFT of $p_{\text{dot}}(\mathbf{x})$ defined as

$$\begin{aligned} P_{\text{dot}}(\mathbf{u}) &= \int_{-\infty}^{\infty} p_{\text{dot}}(\mathbf{x}) e^{-j2\pi\mathbf{u}^T\mathbf{x}}\, d\mathbf{x}\,, \\ &= R^2\text{sinc}(R\mathbf{u})\,, \\ &= \text{sinc}(Ru)\text{sinc}(Rv)\,, \end{aligned} \tag{11}$$

and $\breve{C}(\mathbf{u};a)$ is the Discrete Space Fourier Transform (DSFT) of $c[\mathbf{m};a]$

$$\breve{C}(\mathbf{u};a) = \sum_{\mathbf{m}\in Z^2} c[\mathbf{m};a] e^{-j2\pi\mathbf{u}^T\mathbf{m}}\,. \tag{12}$$

The function $c[\mathbf{m};a]$ in Eq. (12) is the discrete-space halftone dot-cluster function within the fundamental unit halftone cell Ω. It can be expressed as

$$c[\mathbf{m};a] = \begin{cases} 1, & \text{if } a \geq t[\mathbf{m}] \text{ and } \mathbf{m} \in \Omega \\ 0, & \text{else} \end{cases}. \tag{13}$$

To derive the relationship between this halftone image and periodic laser scanner jitter, we view the halftone image $h(\mathbf{x};a)$ as the continuous-tone image $f(x,y)$ in Eq. (1) that is subject to jitter. Then, the Fourier spectrum $F(u,v)$ for the continuous-tone image in Eq. (6) becomes the Fourier spectrum $H(\mathbf{u};a)$ for the halftone image given by Eq. (10). So substituting Eq. (10) into Eq. (6), we obtain

$$\widetilde{H}(\mathbf{u};a) = \sum_k J_k\big(-2\pi[0,A]\mathbf{u}\big) H\left(\mathbf{u} - [k/X,0]^T;a\right)\,, \tag{14}$$

where $\widetilde{H}(\mathbf{u};a)$ denotes the Fourier transform of the continuous-space halftone image with laser scanner jitter.

Evaluation of the Mathematical Model for Laser Scanner Jitter

To evaluate our mathematical model, we compute the Fourier spectrum of a halftone image with scanner jitter (Eq. 14). We then compare the result with the Fourier spectrum of a scanned test target of a 25% tint-fill ($a = \frac{1}{4}$) constant-tone image halftone printed at 600 dpi with two different colorants, black and magenta, using a dry toner laser EP printer. The printed test target is then scanned with an EPSON Expression 10000XL at 2400 dpi. The corresponding periodicity matrices of these two colors are the default design for our target printer. The screen tile vectors for magenta are $\mathbf{n}_1 = [3,-1]^{\text{T}}$ and $\mathbf{n}_2 = [1,3]^{\text{T}}$. For black, they are $\mathbf{n}_1 = [2,-2]^{\text{T}}$ and $\mathbf{n}_2 = [2,2]^{\text{T}}$. The screen frequency for magenta is 190 lpi. For black, it is 212 lpi. The screen angle for magenta is 18 degrees. For black, it is 45 degrees.

Figure 4 shows the scanned images of test targets that are printed with a printer with normal-case and worst-case laser scanners. In our experiment, we swapped the laser scanner assembly in the same printer to eliminate other sources of variability that might be observed from printer to printer. The left column images of Fig. 4 are printed with the normal-case laser scanner. The right column images of Fig. 4 are printed with the worst-case laser scanner. We can see a significant visual difference between the two images in the first row of Fig. 4. However, we do not see a visible difference between the magenta test targets because of the screen angle of the magenta.

To compare the Fourier transform of the scanned images with the analytical results obtained by evaluating Eq. (14), we apply the following processes to the scanned images in Fig. 4(b) and 4(d). First, we transform the scanner RGB to linear RGB by computing the gray balancing curves for the R, G and B channels. To obtain the gray balancing curves, we first scan the 24 neutral gray scale patches on the Kodak Q60 target[†], which is shown in Fig. 3, with an EPSON Expression 10000XL scanner at 2400 dpi. The R, G, and B values for each patch are computed as the average of all the pixel values within each patch. Then, the CIE Y value of each gray scale patch is measure by the X-rite DTP70 Spectrophotometer[‡]. Finally, the gray balancing curves can be approximated by a power law equation as follows

$$R_l = a(R/255)^b + c\,, \tag{15}$$

where $R_l = Y/100$, and R_l is the linearized R output value for a patch. Similarly, we can also find the parameters, a, b, and c for the G and B channels.

Next, we find the transformation matrix for transforming the linear RGB values to CIE XYZ values. We use the process mentioned above to obtain the linear RGB values for the 228 color patches on the Kodak Q60 target. Then, the transformation matrix, M, is given by

$$M = (A^T A)^{-1} A^T X, \quad (16)$$

where matrix A (228×3) contains the 228 linear RGBs, and matrix X (228×3) contains the corresponding CIE XYZ values. Based on the above processing, Fig. $4(b)$ and $4(d)$ are tranformed to CIE XYZ. Finally, the CIE Y values are scaled to range from 0 (black) to 255 (white). We call the scanned Y image processed as described above the luminance image.

Subsequently, we compute the 2D Discrete Fourier Transform (DFT) of the luminance image. However, there are vertical and horizontal line smears, and noise in the frequency spectrum of the luminance image. These artifacts are not accounted for by our analytical result obtained by evaluating Eq. (14). The vertical and horizontal line smears may be due to that fact that the size of the luminance image is a non-integer multiple of periods of the halftone pattern. To eliminate the smears, a raised-cosine window function is applied to the luminance image. This window function drops from 1 to 0 within a zone inside each boundary of the image that comprises 5% of the total width or height of the image. In our experiment, we only apply this window function to the black color luminance image because the DFT of the magenta color luminance image does not show obvious vertical and horizontal line smears. The noise may be introduced by the printing and scanning processes. To eliminate it, we clip everything below 65% of the peak value to zero. This threshold was chosen empirically. Finally, we multiply the entire spectrum by a constant scale factor that makes the value at the origin the same as that for the analytical spectrum. The final Fourier spectra of the printed and scanned halftone patches are shown in Fig. $5(a)$ and (c).

Figure 5 compares the analytical results obtained by evaluating Eq. (14) to those obtained by computing the thresholded DFT of the windowed luminance image of the black and the luminance image of the magenta. The left column images of Fig. 5 are the thresholded Fourier spectra of the windowed luminance image (black) and the luminance image (magenta). The right column images of Fig. 5 are based on Eq. (14) with the default periodicity matrices. For the computation, we set the values for the parameters in Eq. (14) as follows: $A = 1/1200$ inches, $a = 0.25$ absorptance units, $X = 1/60$ inches, and $R = 1/600$ inches. According to Eq. 14, we will have frequency components where the impulses are located; and an impulse corresponds to a pixel in the plot. To enhance its visibility, we replace each such impulse by a 9×9 square with constant amplitude. The Fourier spectrum of the continuous-space halftone image with laser scanner jitter exhibits replications of the spectrum of the original continuous-space halftone image. Each replication is separated by 60 lpi (lines-per-inch) in the frequency domain with different weights. This is because the period X of the laser scanner jitter is $\frac{10}{600}$ inches. By comparison, the spectrum of the scanned image also shows replications that are separated by 60 lpi.

We can see that the analytical Fourier spectrum of magenta can predict the thresholded spectrum of the luminance image effectively. However, there is some mismatch in black. There are three possible reasons for this issue. First, the instability of the EP process may not reproduce the given test target perfectly. Furthermore, the screen frequency of black is higher than the screen frequency of magenta. Thus, the printed image of magenta would have better print quality. Second, we assume the displacement function to be a sinusoid function. However, the actual displacement is not a perfect sine wave function. Finally, the thresholded Fourier spectrum of the windowed luminance image shows that the spectral peaks roll off more as we move away from the origin than is the case with the analytical spectrum computed using Eq. (14). This could be due to the fact that our analytical model assumes that each printer addressable pixel is the function $\text{rect}(\frac{\mathbf{x}}{R})$. However, the effective spot shape may be larger than it is in our model due to dot gain effects. The above factors may be responsible for the mismatch in the first row of Fig. 5.

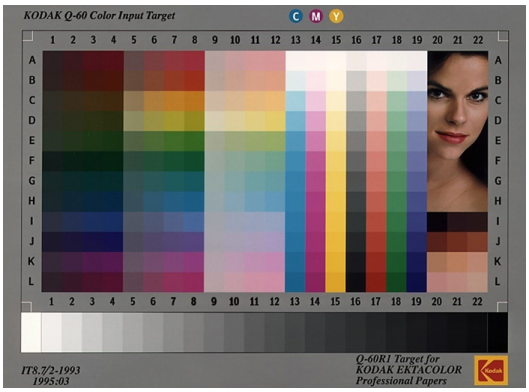

Figure 3. *Kodak Q60 target we used to obtain the gray balancing curves for the R, G and G channels, and the transformation matrix from linear RGB to CIE XYZ*

Conclusions

In this paper, we present a new method for characterizing and analyzing the Fourier spectrum of periodic laser scanner jitter. Unlike prior studies, we incorporate the periodic characteristics of laser scanner jitter into the mathematical model and extend the model to the special case where the jitter has a sinusoidal displacement. This leads to a simple closed-form expression in terms of Bessel functions of the first kind. We further investigate the Fourier domain relationship between a continuous-space halftone image and laser scanner jitter. Our preliminary experimental results shows that the mathematical model can effectively characterize the phenomenon of laser scanner jitter.

References

[1] P-J. Chiang, N. Khanna, A. K. Mikkilineni, M. V. O. Segovia, J. P. Allebach, G T. C. Chiu, and E. J. Delp, "Printer and scanner forensics: models and methods," in Intelligent Multimedia Analysis for Security Applications, Springer-Verlag, 2010, pp. 145-187.

[2] C.-L. Chen, G. T.-C. Chiu, and J. P. Allebach, "Banding reduction in electrophotographic process using human contrast sensitivity function shaped photoreceptor velocity control," Journal of Imaging Science and Technology, vol. 47, 2002, pp. 209-223.

[3] Y. Bang, Z. Pizlo and J. P. Allebach, "Banding assessment with con-

†Eastman Kodak Company, Rochester, NY.
‡X-Rite, Inc., Grand Rapids, MI.

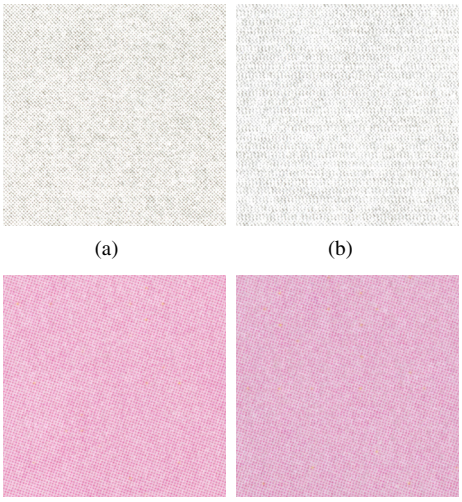

Figure 4. *Comparison of the scanned test targets printed with normal and worst-case laser scanner in two different colorants, black and magenta. (a) The scanned test target printed in black with normal laser scanner. (b) The scanned test target printed in black with worst-case laser scanner. (c) The scanned test target printed in magenta with normal laser scanner. (d) The scanned test target printed in magenta with worst-case laser scanner.*

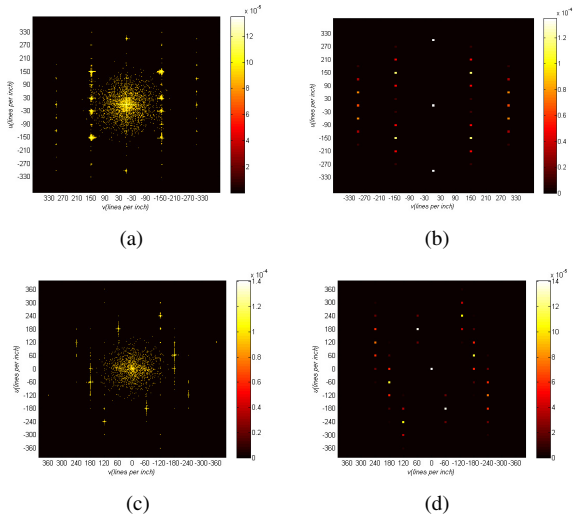

Figure 5. *Comparison of the Fourier spectrum of the scanned test target and the analytical Fourier spectrum both with laser scanner jitter. (a) The thresholded Discrete Fourier Transform of the black color windowed luminance image obtained by the color space transformation of the black color scanned test target in Fig. 4(b) followed by windowing. (b) The result of using Eq. (14) to compute the Fourier spectrum of the continuous-space halftone image with laser scanner jitter using the periodicity matrix for black. (c) The thresholded Discrete Fourier Transform of the magenta color luminance image obtained by the color space transformation of the magenta color scanned test target in Fig. 4(d). (d) The result of using Eq. (14) to compute the Fourier spectrum of the continuous-space halftone image with laser scanner jitter using the periodicity matrix for magenta.*

trolled halftoning: the ten printer experiment," Journal of Imaging Science and Technology, vol. 50, 2006, pp. 522-529.

[4] O. Arslan, Z. Pizlo, and J. P. Allebach, "Softcopy banding visibility assessment," Journal of Imaging Science and Technology, vol. 5, 2007, pp. 271-28.

[5] H. Horikawa, I. Sugisaki, and M. Tashiro, "Relationship between fluctuation in mirror radius (within one polygon) and the jitter," in Proc. SPIE, Beam Deflection and Scanning Technologies, vol. 1454, 1991, pp. 46-59.

[6] G. Stutz, "Eliminating laser scanner artifacts in binary and continuous tone printing," in Proc. SPIE, Micro-Optics/Micromechanics and Laser Scanning and Shaping, vol. 2383, 1995, pp. 427-433.

[7] Ahmed H. Eid, Mohamed N. Ahmed, and Edward E. Rippetoe, "EP printer jitter characterization using 2D Gabor filter and spectral analysis," in Proc. of IEEE Conference on Image Processing, 2008, pp. 1860-1863.

[8] A. H. Eid, M. N. Ahmed, B. E. Cooper, and E. E. Rippetoe, "Characterization of electrophotographic print artifacts: banding, jitter, and ghosting," IEEE Transactions on Image Processing, vol. 20, 2011, pp. 1313-1326.

[9] S. Haykin, Communication systems, Wiley, New York, NY, 2001.

[10] T. S. Rao, G. R. Arce and J. P. Allebach, "Analysis of ordered dither for arbitrary sampling lattices and screen periodicities," IEEE Transactions on Acoustics, Speech, and Signal Processing, vol. 38, 1990, pp. 1981-2000.

Author Biography

Yi-Ting Chen received his B.S. degree in electronics engineering from National Chiao Tung University, Hsinchu, Taiwan, in 2009. He is currently pursuing his Ph.D. degree in electrical and computer engineering at Purdue University. His current research interests include digital image processing, color science, and digital imaging.